Sensor and Simulation Notes

Note 363
December 16, 1993

AXIAL FIELD OF A TEM-FED UWB REFLECTOR ANTENNA: THE PO/PTD CONSTRUCTION

Y. RAHMAT-SAMII and D. W. DUAN

Department of Electrical Engineering
University of California, Los Angeles
Los Angeles, CA 90024-1594

ABSTRACT

Proper characterization of the radiated field along the axial direction of a TEM-fed symmetric paraboloid reflector antenna is important for assessing the impulse response performance of these antennas. The challenging issues in this task is the evaluation of the edge diffracted fields from the rim of the reflector and the spherical TEM-launcher's blades. It is the objective of this study to investigate the effect of the edge diffracted field of the reflector and the scattering from the TEM-launcher's blades using PO/PTD diffraction techniques. As a result, with a general spherical incident field representation, closed-form formulas are obtained for both the PO field and the PTD fringe field of the reflector and the transverse blades. Useful information are extracted from the results. A specialization of these results to a prescribed radiation characteristic of the TEM-launcher is also considered.

Nomenclature and list of symbols

All vectors are represented by boldface symbols except the unit vectors, which are represented by Italic symbols topped with a hat such as $\hat{n}$. Three types of coordinate systems are used in this report: the antenna coordinate system (ACS), the feed coordinate system (FCS), and the local coordinate systems (LCS) defined for each point on the edge of the reflector and the edges of the TEM-launcher's blades. Quantities that has a subscript "f" are related to the FCS. Primed symbols are related to the LCS, except that $\mathbf{r}'$ in the radiation integrals refers to the position of a source point.

$\mathbf{E}, \mathbf{H}$	electric and magnetic fields
$\mathbf{r}$	the position vector of an observation point
$\hat{n}$	a unit vector normal to the surface of the reflector or that of a blade, pointing to the incident wave
θ, ϕ	polar and azimuthal angles in ACS
θ_f, ϕ_f	polar and azimuthal angles in FCS
θ_i', ϕ_i'	polar and azimuthal angles, in LCS, of an incident ray
θ', ϕ'	polar and azimuthal angles, in LCS, of an observation point
$\hat{\theta}$, $\hat{\phi}$	(spherical) unit vectors in ACS
$\hat{\theta}_f$, $\hat{\phi}_f$	(spherical) unit vectors in FCS
$\hat{\theta}_i'$, $\hat{\phi}_i'$	(spherical) unit vectors, in LCS, associated with an incident ray
$\hat{\theta}'$, $\hat{\phi}'$	(spherical) unit vectors, in LCS, associated with an observation point
D, F	the diameter and focal length of a symmetric paraboloidal reflector
θ_s	the subtended angle of the reflector
F_θ, G_θ, G_ϕ	diffraction coefficients of PTD
$\mathbf{E}^{\text{inc}}_{\theta_i'}$, $\mathbf{H}^{\text{inc}}_{\theta_i'}$	the $\hat{\theta}_i'$-components of the incident field
E_{θ_f}, E_{ϕ_f}	the $\hat{\theta}_f$- and $\hat{\phi}_f$-components of the feed electric field
ρ, ψ	the reflector aperture parameters
UWB	Ultra Wide Band
PO	Physical Optics
PTD	Physical Theory of Diffraction
GO	Geometrical Optics

Chapter 1

Introduction

The goal of this study is to determine the axial-field of a TEM-fed symmetric paraboloid reflector antenna for ultra wide band (UWB) radar applications. An example of the TEM-fed reflector antenna is depicted in Figure 1.1, in which the TEM-launcher is assumed to have four blades although in practice other numbers of the blades may be used. In order to accurately predict the performance of the TEM-fed antennas, it is necessary to characterize not only the scattered field of the reflector, but also that of the TEM-launcher's blades. The diffraction techniques of Physical Optics (PO) and Physical Theory of Diffraction (PTD) [1, 2, 3] are chosen for analysis because they are accurate and versatile.

The general formulation of PO/PTD is presented in Chapter 2. This technique is applied to characterize the scattered field of the reflector in Chapter 3, and that of the TEM-launcher's blades in Chapter 4. As a result, with a general spherical incident field representation, closed-form formulas are obtained for various axial field components. These formulas provide useful information on the diffraction effects of the reflector edge and the launcher's blades, and will facilitate the characterization of the time-domain response of these reflector antenna systems.

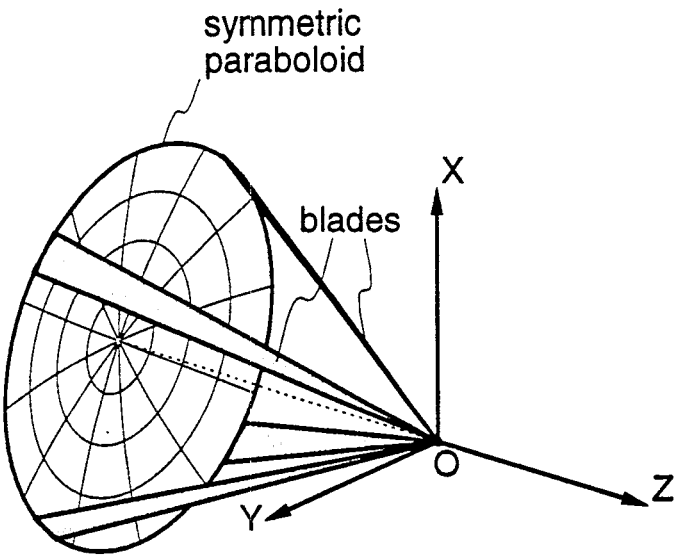

Figure 1.1: A possible configuration of the TEM-fed reflector antenna. It is assumed in this drawing that the TEM-launcher has four blades although in practice other numbers of the blades may be used.

Chapter 2

PO/PTD diffraction analysis

Consider the scattering problem shown in Figure 2.1, in which a scatterer with a curved edge is being illuminated by an incident field. It is assumed that the scatterer is electrically large that the method of moments is not easily applicable to obtain the numerically exact solution for the scattered field. Analysis of reflector antennas, for example, falls into this category for typical applications. In this situation, one has to resort to approximate methods. We will focus on the application of the high frequency diffraction techniques such as Physical Optics (PO) and Physical Theory of Diffraction (PTD) to the TEM-fed reflector antennas in this report. The general formulation of the PO/PTD analysis is summarized in Section 2.1 and Section 2.2. For purpose of presenting a readily applicable formulation, special attention is given to the definitions of the elements that are required to construct the PO field and the PTD fringe field. The time convention $e^{j\omega t}$ is assumed and suppressed. All formulas are presented for observations made in far-field zone.

2.1 Physical Optics

In Physical Optics, the current on the scatterer surface is assumed to be

$$\mathbf{J}^{\mathrm{PO}} = \begin{cases} 2\hat{n} \times \mathbf{H}^{\mathrm{inc}}, & \text{in the lit region} \\ 0, & \text{in the dark region} \end{cases} \tag{2.1}$$

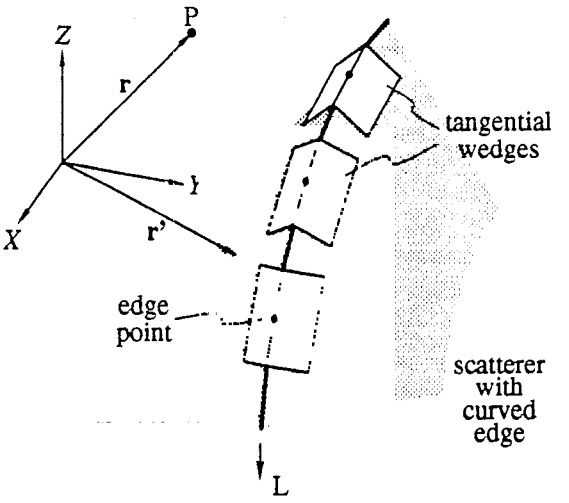

Figure 2.1: A scatterer with curved edge and the local tangential wedges.

The PO scattered field, $\mathbf{E}^{\mathrm{PO}}$, is generated by the PO surface current $\mathbf{J}^{\mathrm{PO}}$:

$$\mathbf{E}^{\mathrm{PO}}(\mathbf{r}) = -jkZ_0\frac{e^{-jkr}}{4\pi r}(\hat{\hat{\mathbf{I}}} - \hat{r}\hat{r}) \cdot \int_{\Sigma} \mathbf{J}^{\mathrm{PO}}(\mathbf{r}')e^{jk\hat{r}\cdot\mathbf{r}'}d\Sigma \tag{2.2}$$

$$\mathbf{H}^{\mathrm{PO}}(\mathbf{r}) = \frac{1}{Z_0}\hat{r} \times \mathbf{E}^{\mathrm{PO}} \tag{2.3}$$

$$k = \omega\sqrt{\mu_0\epsilon_0}, \quad Z_0 = \sqrt{\frac{\epsilon_0}{\mu_0}} \tag{2.4}$$

where k is the free space wave number, Z_0 is the free space impedance, and the operation $(\hat{\hat{\mathbf{I}}} - \hat{r}\hat{r})$ in (2.2) is read "the transverse-to-$\hat{r}$ components of".

2.2 Physical Theory of Diffraction

The PO field (2.2) and (2.3) has taken into consideration part of the diffraction effect caused by the edge of the scatterer. In order to improve the accuracy of PO, the other portion of the edge diffracted field is modeled by a "fringe field" in the Physical Theory of Diffraction using asymptotic techniques. The total scattered field in PTD consists of the PO field and the fringe field:

$$\mathbf{E}^s = \mathbf{E}^{\mathrm{PO}} + \mathbf{E}^{\mathrm{fr}} \tag{2.5}$$

The key idea of PTD is as follows. It is assumed in PTD that, in the high frequency regime, edge scattering is a local phenomenon, and therefore the diffracted field of a curved edge can be approximated by the sum of those contributed by the differential edge elements. Based on the same locality principle, each edge element is modeled by a local tangential straight wedges (see Figure 2.1). With these assumptions, the problem of determining the edge diffraction of a scatterer that has an arbitrarily curved edge is reduced to that of a straight wedge, which is a canonical problem with exact solution. The key issue of PTD is to obtain a high frequency asymptotic development of the fringe field radiated from a differential edge element of a straight wedge (the "Elementary Edge Wave" by Ufimtsev).

In this report, the PTD of [1, 2, 3] is extended to the whole angular range of $[0, 2\pi]$ for the incident azimuthal direction. This extension is valuable for practical applications because the restriction on the orientations of the local coordinate systems is lifted. In order to facilitate PO/PTD analysis of reflector antennas, the general PTD fringe field formulas are specialized to *scatterers with thin edges*, and the resultant fringe fields $\mathbf{E}^{\mathrm{fr}}$ and $\mathbf{H}^{\mathrm{fr}}$ are:

$$\mathbf{E}^{\mathrm{fr}}(\mathbf{r}) = \frac{e^{-jkr}}{4\pi r}\int_L \left[\hat{\theta}'(\mathbf{E}^{\mathrm{inc}}_{\theta'_i}F_\theta + Z_0\mathbf{H}^{\mathrm{inc}}_{\theta'_i}G_\theta) + \hat{\phi}' Z_0\mathbf{H}^{\mathrm{inc}}_{\theta'_i}G_\phi\right] e^{jk\hat{r}\cdot\mathbf{r}'}dl \qquad (2.6)$$

$$\mathbf{H}^{\mathrm{fr}}(\mathbf{r}) = \frac{1}{Z_0}\hat{r}\times\mathbf{E}^{\mathrm{fr}} \qquad (2.7)$$

where F_θ, G_θ, and G_ϕ are usually referred to as the "diffraction coefficients". Notice that a prime is attached to the unit vectors in (2.6) in order to emphasize that these vectors are defined with respect to each local coordinate system, and may vary along the edge of the scatterer. The fields $\mathbf{E}^{\mathrm{inc}}_{\theta'_i}$ and $\mathbf{H}^{\mathrm{inc}}_{\theta'_i}$ are also defined with respect to the local coordinate systems. The integrals in (2.6) and (2.7) are one-dimensional, along the curved scatterer edge L. Compared to the two-dimensional PO integral

performed over the scatterer's surface, the fringe field integrals only increase the computation time marginally. The diffraction coefficients are functions of the angles of the incident waves (the "incident angles" θ_i' and ϕ_i') and those of the observation point (the "observation angles" θ' and ϕ'). Precisely,

$$F_\theta = \frac{\sin\theta'}{\sin\theta_i'} \frac{-2\sin\frac{\phi_i'}{2}}{\cos\frac{\sigma}{2} + \left|\cos\frac{\phi_i'}{2}\right|} \tag{2.8}$$

$$G_\theta = -\epsilon(\phi_i') \frac{\cos\theta'\cos\phi' + \frac{\sin\theta'}{\sin\theta_i'}\cos\theta_i'\left(1 + 2\cos\frac{\sigma}{2}\left|\cos\frac{\phi_i'}{2}\right|\right)}{\cos\frac{\sigma}{2}\left(\cos\frac{\sigma}{2} + \left|\cos\frac{\phi_i'}{2}\right|\right)} \tag{2.9}$$

$$G_\phi = \frac{\epsilon(\phi_i')\sin\phi'}{\cos\frac{\sigma}{2}\left(\cos\frac{\sigma}{2} + \left|\cos\frac{\phi_i'}{2}\right|\right)} \tag{2.10}$$

$$\epsilon(\phi_i') = \begin{cases} 1, & \phi_i' < \pi \\ 0, & \phi_i' = \pi \\ -1, & \phi_i' > \pi \end{cases} \tag{2.11}$$

$$\cos\sigma = -\mu \tag{2.12}$$

$$\mu = \frac{\sin\theta'\cos\phi' - \cot\theta_i'(\cos\theta' + \cos\theta_i')}{\sin\theta_i'} \tag{2.13}$$

$$\cos\frac{\sigma}{2} = \begin{cases} \sqrt{\frac{1-\mu}{2}}, & -1 \le \mu \le 1 \\ -\frac{j}{2}\left(A - \frac{1}{A}\right), & \mu > 1 \\ \frac{1}{2}\left(A + \frac{1}{A}\right), & \mu < -1 \end{cases} \tag{2.14}$$

$$A = \sqrt{|\mu| + \sqrt{\mu^2 - 1}} \tag{2.15}$$

where the incident angles θ_i' and ϕ_i', and the observation angles θ' and ϕ' are defined with respect to the local coordinate system associated with each edge element along the curved edge of the scatterer. The definitions of the incident and observation angles are depicted in Figure 2.2, in which it is seen that for a thin scatterer the local tangential wedge is simply a half plane, and that the z-axis of the local coordinate

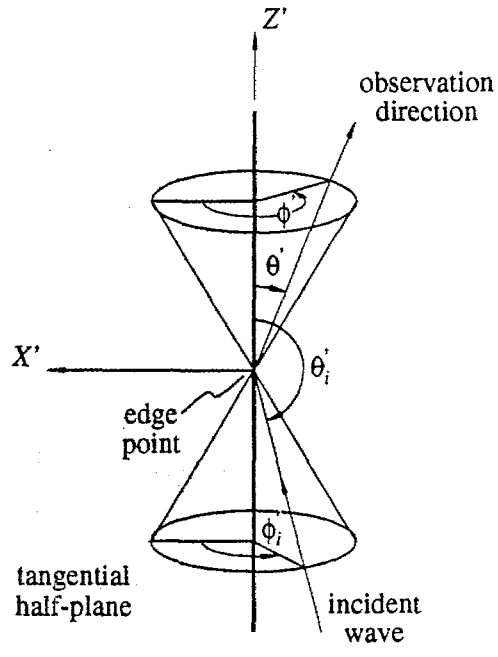

Figure 2.2: The incident angles and observation angles that are required in the calculation of the PTD fringe field.

system is defined to be tangential to the edge of the scatterer, while the x-axis is situated on the tangential half plane, pointing "inward" at a right angle to the edge. As an example, the diffraction coefficients for incident angles $\theta_i' = 60°$ and $\phi_i' = 80°$ are plotted in Figure 2.3.

2.3 PO/PTD field for axial observation

In reflector antenna analysis, the z-axis is usually defined to be along the boresight or the axis of the antenna. This convention is used in this report.

When the observation is made along the axis of the antenna at

$$\mathbf{r} = \hat{z}r \tag{2.16}$$

we have $\hat{r} = \hat{z}$ and the general far-field formulas (2.2) and (2.3) reduce to

$$\mathbf{E}^{\mathrm{PO}}(\mathbf{r}) = -jkZ_0\frac{e^{-jkr}}{4\pi r}(\hat{x}\hat{x} + \hat{y}\hat{y}) \cdot \int_{\Sigma} \mathbf{J}^{\mathrm{PO}}\, e^{jk\hat{z}\cdot\mathbf{r}'} d\Sigma \tag{2.17}$$

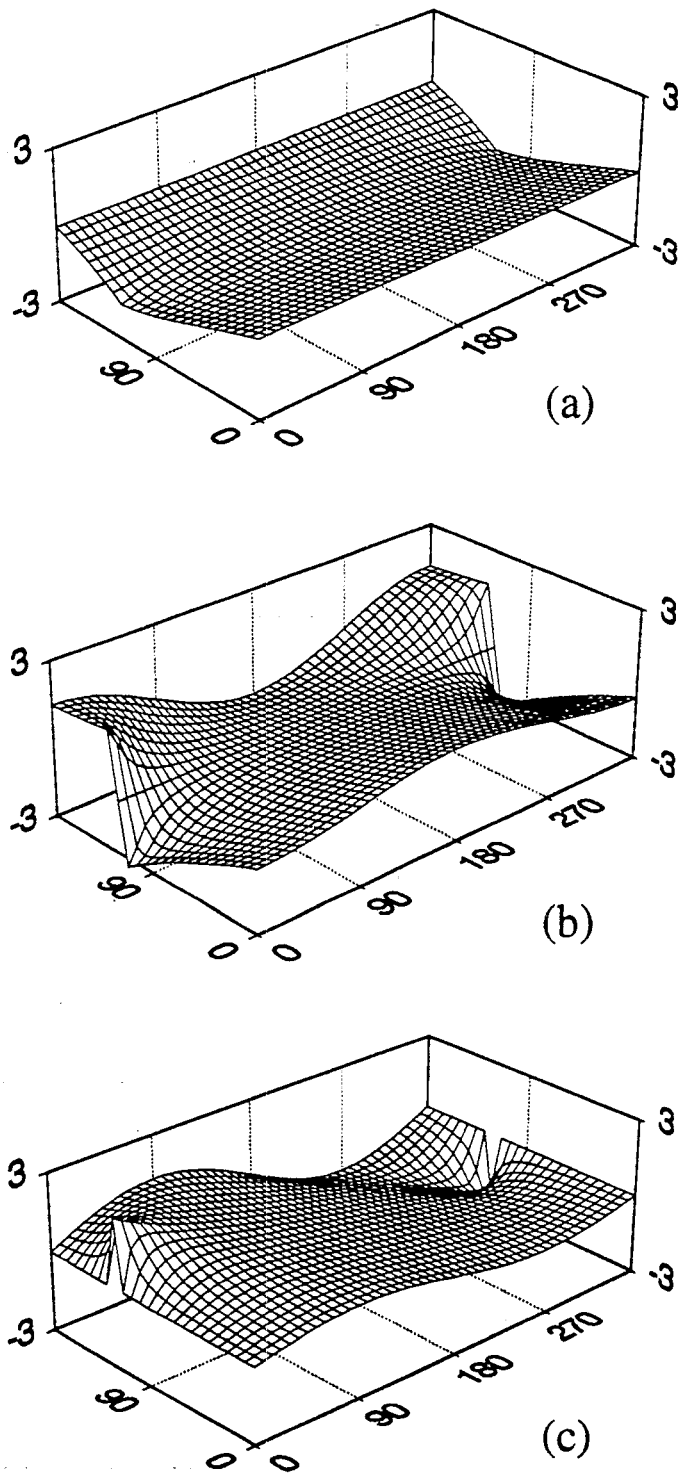

Figure 2.3: PTD diffraction coefficients for $\theta_i' = 60°$ and $\phi_i' = 80°$. (a) F_θ. (b) G_θ. (c) G_ϕ. The diffraction coefficients are plotted for $\theta' \in [0, 180°]$ and $\phi' \in [0, 360°]$

$$\mathbf{H}^{\mathrm{PO}}(\mathbf{r}) = \frac{1}{Z_0}\hat{z} \times \mathbf{E}^{\mathrm{PO}} \tag{2.18}$$

These equations define the axial PO fields that are of our interest. Notice that the surface Σ may represent the reflector surface or that of the TEM-launcher's blades.

Similarly, the fringe fields (2.6) and (2.7) can also be simplified for axial observation:

$$\mathbf{E}^{\mathrm{fr}}(\mathbf{r}) = \frac{e^{-jkr}}{4\pi r}\int_L \left[\hat{\theta}'(\mathbf{E}^{\mathrm{inc}}_{\theta'_i}F_\theta + Z_0\mathbf{H}^{\mathrm{inc}}_{\theta'_i}G_\theta) + \hat{\phi}' Z_0\mathbf{H}^{\mathrm{inc}}_{\theta'_i}G_\phi\right] e^{jk\hat{z}\cdot\mathbf{r}'}dl \tag{2.19}$$

$$\mathbf{H}^{\mathrm{fr}}(\mathbf{r}) = \frac{1}{Z_0}\hat{r} \times \mathbf{E}^{\mathrm{fr}} \tag{2.20}$$

The edge L may represent that of the reflector or the edges of the TEM-launcher's blades depending on the context of application.

Chapter 3

Analysis of the reflector

The previously published asymptotic formulas for the PO field of symmetric (body of revolution) reflector antennas [4, 5, 6] are singular for boresight (the axial direction) observation, and are not useful for solving our problem. In this chapter, the PO/PTD diffraction technique presented in Chapter 2 is applied to determine the axial field of a symmetric paraboloidal reflector. Closed-form formulas are derived for both the PO field of the reflector and the fringe field from the edge of the reflector.

3.1 Axial PO field in closed-form

Let us consider the reflector antenna geometry Figure 3.1, in which a symmetric paraboloidal reflector (denoted by "Σ") with a circular aperture (denoted by "A") is illuminated by a feed situated at the focal point of the paraboloid.

The steps that lead to the closed-form evaluation of the integrals in (2.17) are detailed in the following.

3.1.1 The feed and the coordinate systems

There are two coordinate systems in the geometry shown in Figure 3.1: the antenna coordinate system $C = \{\hat{x}, \hat{y}, \hat{z}\}$ and the feed coordinate system $C = \{\hat{x}_f, \hat{y}_f, \hat{z}_f\}$, with the origins of both systems situated at the focal point of the paraboloid. The

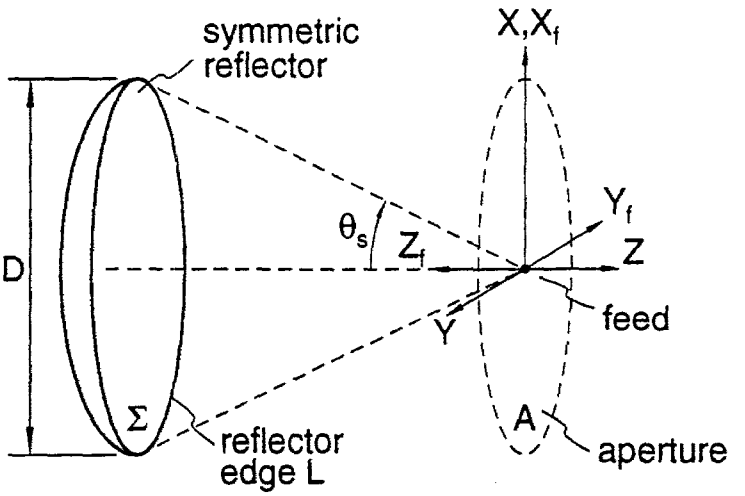

Figure 3.1: Antenna geometry and the coordinate systems.

unit vectors of the two systems are related by

$$\hat{x}_f = \hat{x}, \quad \hat{y}_f = -\hat{y}, \quad \hat{z}_f = -\hat{z} \tag{3.1}$$

A point on the reflector surface can be represented either by the C-coordinates (x, y, z) or the C_f-coordinates (x_f, y_f, z_f). These coordinates are related by

$$x_f = x, \quad y_f = -y, \quad z_f = -z \tag{3.2}$$

The spherical coordinate systems, $S = \{\hat{r}, \hat{\theta}, \hat{\phi}\}$ and $S_f = \{\hat{r}_f, \hat{\theta}_f, \hat{\phi}_f\}$, that correspond to C and C_f respectively can also be related in a similar manner:

$$\hat{r}_f = \hat{r}, \quad \hat{\theta}_f = -\hat{\theta}, \quad \hat{\phi}_f = -\hat{\phi} \tag{3.3}$$

$$r_f = r, \quad \theta_f = \pi - \theta, \quad \phi_f = -\phi, \tag{3.4}$$

The feed coordinate systems are convenient in describing the field radiated by the feed. In this study, we assume the feed pattern:

$$\mathbf{E}^{\text{feed}} = \frac{e^{-jkr_f}}{r_f}\left[\hat{\theta}_f E_{\theta_f}(\theta_f, \phi_f) + \hat{\phi}_f E_{\phi_f}(\theta_f, \phi_f)\right] \tag{3.5}$$

$$\mathbf{H}^{\text{feed}} = \frac{1}{Z_0}\hat{r}_f \times \mathbf{E}^{\text{feed}} \tag{3.6}$$

With the help of (3.3) and (3.4), one obtains the incident fields on the reflector:

$$\mathbf{E}^{\text{inc}} = -\frac{e^{-jkr}}{r}\left[\hat{\theta}\, E_{\theta_f}(\pi-\theta,-\phi)+\hat{\phi}\, E_{\phi_f}(\pi-\theta,-\phi)\right] \tag{3.7}$$

$$\mathbf{H}^{\text{inc}} = \frac{1}{Z_0}\frac{e^{-jkr}}{r}\left[-\hat{\phi}\, E_{\theta_f}(\pi-\theta,-\phi)+\hat{\theta}\, E_{\phi_f}(\pi-\theta,-\phi)\right] \tag{3.8}$$

Equation (3.8) will be used in the next section to construct the PO current. Notice that E_{θ_f} and E_{ϕ_f} are the feed pattern functions in unit of volts.

3.1.2 PO current and the Jacobian

Let us assume that the reflector surface is described by the function

$$z = f(x,y) \tag{3.9}$$

It is convenient to evaluate the integral in (2.17) using the variables defined on the planar aperture A [7]. For example, one may use ρ and ψ, which are related to the Cartesian coordinates by $x=\rho\cos\psi$, $y=\rho\sin\psi$. In this situation, the area element $d\Sigma$ in (2.17) has to be replaced by

$$d\Sigma = \mathcal{J}\rho d\psi d\rho \tag{3.10}$$

where

$$\mathcal{J} = \left[\left(\frac{\partial f}{\partial x}\right)^2+\left(\frac{\partial f}{\partial y}\right)^2+1\right]^{1/2} \tag{3.11}$$

is the Jacobian. The unit vector that is normal to the reflector surface and points to the illuminated side of the reflector is

$$\hat{n} = \mathcal{J}^{-1}\cdot\left[\hat{x}\left(-\frac{\partial f}{\partial x}\right)+\hat{y}\left(-\frac{\partial f}{\partial y}\right)+\hat{z}\right] \tag{3.12}$$

For a symmetric reflector, equations (3.11) and (3.12) can be further reduced to

$$\mathcal{J} = \left[\left(\frac{\partial f}{\partial \rho}\right)^2+1\right]^{1/2} \tag{3.13}$$

$$\hat{n} = \mathcal{J}^{-1}\cdot\left[\hat{x}\left(-\cos\psi\frac{\partial f}{\partial \rho}\right)+\hat{y}\left(-\sin\psi\frac{\partial f}{\partial \rho}\right)+\hat{z}\right] \tag{3.14}$$

With the help of (3.14) and (3.8), it is easy to show that the PO current (2.1) for a symmetric reflector can be written as

$$\mathbf{J}^{\mathrm{PO}} = \mathcal{J}^{-1} \cdot \frac{2}{Z_0} \cdot \frac{e^{-jkr}}{r} \left(\hat{x} J_x^{\mathrm{PO}} + \hat{y} J_y^{\mathrm{PO}} + \hat{z} J_z^{\mathrm{PO}} \right) \tag{3.15}$$

$$J_x^{\mathrm{PO}} = \left(\sin\theta \sin\phi \frac{\partial f}{\partial \rho} - \cos\theta \sin\phi \right) \cdot E_{\phi_f} + \cos\phi \cdot E_{\theta_f} \tag{3.16}$$

$$J_y^{\mathrm{PO}} = \left(-\sin\theta \cos\phi \frac{\partial f}{\partial \rho} + \cos\theta \cos\phi \right) \cdot E_{\phi_f} + \sin\phi \cdot E_{\theta_f} \tag{3.17}$$

$$J_z^{\mathrm{PO}} = \frac{\partial f}{\partial \rho} \cdot E_{\theta_f} \tag{3.18}$$

It must be mentioned that the coordinates r, θ, ϕ in the above equations refer to a point on the reflector surface. When used in (2.17), however, a surface point becomes a "source" point, and symbols that are more suitable for representing a source point should be used in place of r, θ, ϕ in order to avoid confusion with the coordinates of an observation point.

3.1.3 Axial PO field of a symmetric paraboloid

Applying (3.10) and (3.15) to a symmetric paraboloid with focal length F and diameter D:

$$z = -F + \frac{x^2 + y^2}{4F} \tag{3.19}$$

one obtains the specialization of (2.17):

$$\mathbf{E}_{\mathrm{refl}}^{\mathrm{PO}} = -jkF \frac{e^{-jk(r+2F)}}{r} \cdot \int_{\cos\theta_s}^{1} \frac{1}{\pi} \int_0^{2\pi} \left(\hat{x} J_x^{\mathrm{PO}} + \hat{y} J_y^{\mathrm{PO}} \right) d\psi \frac{d\cos\theta_f}{1 + \cos\theta_f} \tag{3.20}$$

where

$$\theta_s = 2 \arctan \frac{D}{4F} \tag{3.21}$$

is the subtended angle of the reflector (see Figure 3.1). To further reduce (3.20), a feed radiation pattern must be assumed. For example, using the feed model

$$\mathbf{E}^{\text{feed}} = \frac{e^{-jkr_f}}{r_f} \cdot \begin{cases} \left[\hat{\theta}_f A(\theta_f)\cos\phi_f - \hat{\phi}_f B(\theta_f)\sin\phi_f\right], & x\text{-pol feed} \\ \left[\hat{\theta}_f A(\theta_f)\sin\phi_f + \hat{\phi}_f B(\theta_f)\cos\phi_f\right], & y\text{-pol feed} \\ \frac{e^{-j\phi_f}}{\sqrt{2}}\left[\hat{\theta}_f A(\theta_f) - \hat{\phi}_f jB(\theta_f)\right], & \text{RHCP feed} \\ \frac{e^{j\phi_f}}{\sqrt{2}}\left[\hat{\theta}_f A(\theta_f) + \hat{\phi}_f jB(\theta_f)\right], & \text{LHCP feed} \end{cases} \tag{3.22}$$

in (3.20), one obtains

$$\mathbf{E}^{\text{PO}}_{\text{refl}} = \hat{p} \cdot \frac{e^{-jk(r+2F)}}{r} \cdot (-jkF) \cdot \underbrace{\int_{\cos\theta_s}^{1} \frac{A(\theta_f) + B(\theta_f)}{1+\cos\theta_f} d(\cos\theta_f)}_{I} \tag{3.23}$$

where

$$\hat{p} = \begin{cases} \hat{x}, & x\text{-pol feed} \\ -\hat{y}, & y\text{-pol feed} \\ \frac{\hat{x}+j\hat{y}}{\sqrt{2}}, & \text{RHCP feed} \\ \frac{\hat{x}-j\hat{y}}{\sqrt{2}}, & \text{LHCP feed} \end{cases} \tag{3.24}$$

is the polarization vector. Notice that the sense of circular polarization has been reverted upon reflection from the reflector. The integral I in (3.23) is easy to evaluate numerically since it has a slowly varying integrand and a finite integration interval. Nevertheless, there are several functional forms of $A(\theta_f)$ and $B(\theta_f)$ that allow closed-form evaluation of I. For example, when the $\cos^q\theta$ feed model is used:

$$A(\theta_f) = (\cos\theta_f)^{q_1}, \quad B(\theta_f) = (\cos\theta_f)^{q_2} \tag{3.25}$$

one may use the formula [8]

$$\int \frac{\tau^n}{1+\tau} d\tau = \frac{\tau^n}{n} - \frac{\tau^{n-1}}{n-1} + \frac{\tau^{n-2}}{n-2} - \cdots + (-1)^{n-1}\tau + (-1)^n \log(1+\tau) \tag{3.26}$$

to calculate I for integer q's.

The validity of (3.23) can be justified in two ways. Firstly, we find that for large focal length F, equation (3.23) is consistent with a closed-form formula previously

derived for the axial field of a circular disc that has uniformly distributed surface current. This comparison is detailed in Appendix A. Secondly, the field computed using (3.23) is compared with the result obtained by numerical integration. For example, using the antenna configuration $D = 10\lambda$, $F = 5\lambda$, and an x-polarized $\cos^q\theta$ feed with $q_1 = 4.3$, and $q_2 = 2.8$, one obtains $\mathbf{E}^{\mathrm{PO}}_{\mathrm{refl}} = -\hat{x}j0.606 \times 10^{-5}\mathrm{volts}/\lambda$ at the point $\hat{r} = \hat{z}10^6\lambda$. It is observed that the amplitude of the axial PO field (3.23) has k^1-dependence, which becomes singular at the high frequency limit ($k \to \infty$). This behavior is consistent with that predicted by the Geometrical Optics (GO). Equation (3.23) provides a more accurate quantitative characterization of this singularity. To further illustrate the k^1-dependence of the axial PO field, a paraboloidal reflector with $D = 1$ m and $F/D = 0.4$ is analyzed over a frequency band, and the result is plotted in Figure 3.3.

3.2 Reflector edge diffracted field

The PTD fringe field along the axial direction of a symmetric paraboloidal reflector is evaluated in this section.

To specialize these general formulas for a paraboloidal antenna, consider the geometry depicted in Figure 3.2, in which F is the focal length and D is the diameter of the paraboloid. The edge of the reflector is indexed by the angular parameter ψ, and a local coordinate system $C' = \{\hat{x}', \hat{y}', \hat{z}'\}$ is erected for each edge point P' in the manner as depicted in Figure 3.2. The observation point P is situated on the z-axis, at a large distance r from the origin. In the following, elements in the integrand of (2.19) are considered in sequence.

- *The phase factor* $e^{jk\hat{z}\cdot\mathbf{r}'}$: Since the rim of the reflector share the common z-

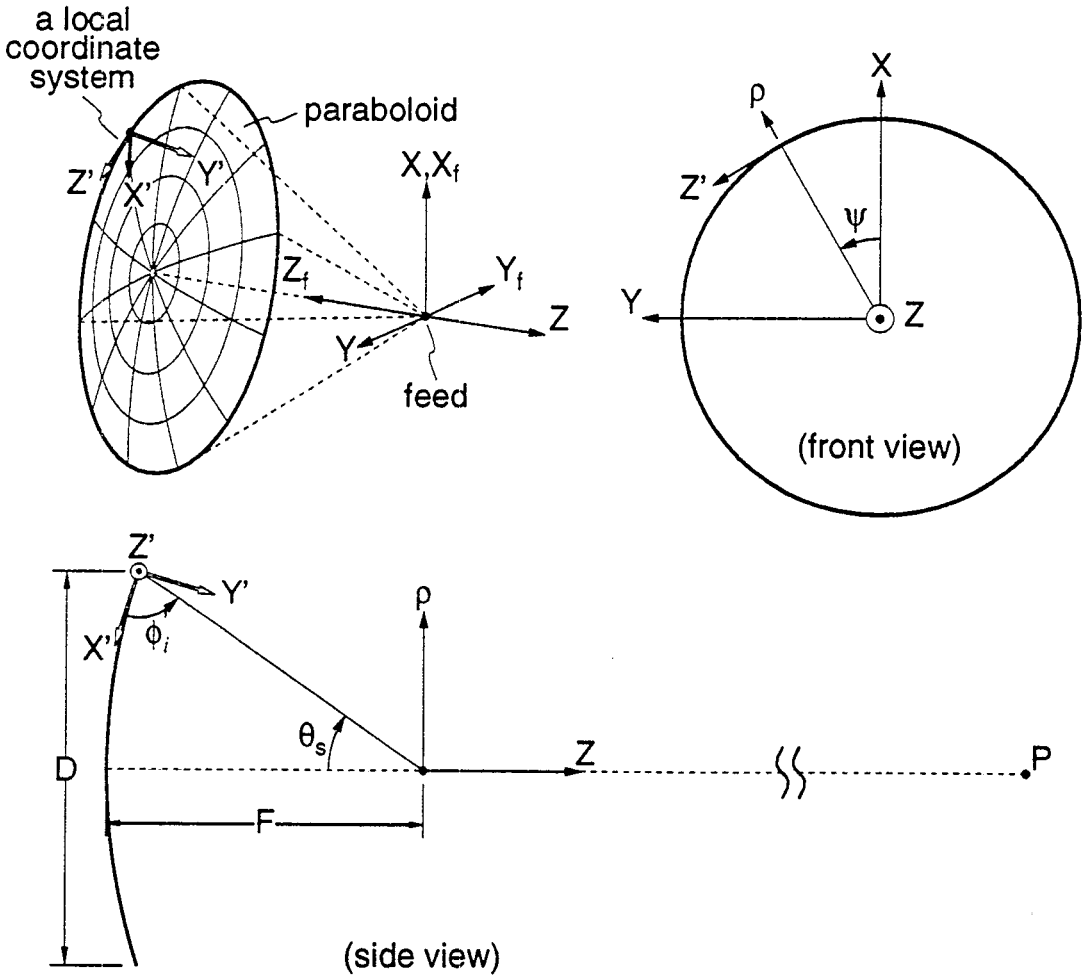

Figure 3.2: Geometry of the local coordinate systems for a symmetric paraboloidal antenna.

coordinate

$$z_0 = -F \cdot m_- \tag{3.27}$$

$$m_- \equiv 1 - \left(\frac{D}{4F}\right)^2 \tag{3.28}$$

the phase factor $e^{-jk\hat{z}\cdot\mathbf{r}'}$ in (2.17) has the *constant* value e^{jkz_0}.

- *The incident and observation angles*: It is easy to show, using the geometry of Figure 3.2, that the incident angles (with respect to the local coordinate system C') of the ray field coming from the focal point of the paraboloid are

$$\theta_i' = \frac{\pi}{2}, \quad \phi_i' = \frac{\pi}{2} - \frac{\theta_s}{2} \tag{3.29}$$

and the observation angles (again, with respect to the local coordinate system C') are

$$\theta' = \frac{\pi}{2}, \quad \phi' = \frac{\pi}{2} + \frac{\theta_s}{2} \tag{3.30}$$

where θ_s is the subtended angle of the reflector and has been defined in (3.21).

- *The diffraction coefficients*: Applying (3.29) and (3.30) to equations (2.8), (2.9), and (2.10), one obtains the diffraction coefficients:

$$-F_\theta = G_\phi = \frac{1 - \sin\frac{\theta_s}{2}}{\cos\frac{\theta_s}{2}}, \quad G_\theta = 0 \tag{3.31}$$

- *The unit vectors $\hat{\theta}'$ and $\hat{\phi}'$*: $\hat{\theta}'$ and $\hat{\phi}'$ in (2.19) are unit vectors evaluated at P from the point of view of the local coordinate system C'. For a rim point P' that has the coordinates

$$\mathbf{r}' = \hat{x}\frac{D}{2}\cos\psi + \hat{y}\frac{D}{2}\sin\psi + \hat{z}z_0 \tag{3.32}$$

it is seen that

$$\hat{\theta}' = \hat{x}\sin\psi - \hat{y}\cos\psi \tag{3.33}$$

$$\hat{\phi}' = \hat{x}\cos\psi + \hat{y}\sin\psi \tag{3.34}$$

- *The incident fields*: Let r_0 be the focus-to-rim distance:

$$r_0 = F \cdot m_+ \tag{3.35}$$

$$m_+ \equiv 1 + \left(\frac{D}{4F}\right)^2 \tag{3.36}$$

The incident field for an edge point that has the spherical coordinates $(r, \theta, \phi) = (r_0, \pi - \theta_s, \psi)$ can be obtained from (3.7) and (3.8):

$$\mathbf{E}^{\text{inc}} = -\frac{e^{-jkr}}{r}\left[\hat{\theta}E_{\theta_f}(\theta_s, -\psi) + \hat{\phi}E_{\phi_f}(\theta_s, -\psi)\right] \tag{3.37}$$

$$\mathbf{H}^{\text{inc}} = \frac{1}{Z_0}\frac{e^{-jkr}}{r}\left[-\hat{\phi}E_{\theta_f}(\theta_s, -\psi) + \hat{\theta}E_{\phi_f}(\theta_s, -\psi)\right] \tag{3.38}$$

$$\hat{\theta} = -\hat{x}\cos\theta_s\cos\psi - \hat{y}\cos\theta_s\sin\psi - \hat{z}\sin\theta_s \tag{3.39}$$

$$\hat{\phi} = -\hat{x}\sin\psi + \hat{y}\cos\psi \tag{3.40}$$

The inner products of these incident fields with the unit vector

$$\hat{\theta}_i' = \hat{x}\sin\psi - \hat{y}\cos\psi \tag{3.41}$$

give the field components $\mathbf{E}^{\text{inc}}_{\theta_i'}$ and $\mathbf{H}^{\text{inc}}_{\theta_i'}$:

$$\mathbf{E}^{\text{inc}}_{\theta_i'} = \mathbf{E}^{\text{inc}} \cdot \hat{\theta}_i' = \frac{e^{-jkr_0}}{r_0}E_{\phi_f}(\theta_s, -\psi) \tag{3.42}$$

$$\mathbf{H}^{\text{inc}}_{\theta_i'} = \mathbf{H}^{\text{inc}} \cdot \hat{\theta}_i' = \frac{1}{Z_0}\frac{e^{-jkr_0}}{r_0}E_{\theta_f}(\theta_s, -\psi) \tag{3.43}$$

When all these details are assembled together, one arrives at the axial fringe field:

$$\mathbf{E}^{\text{fr}}_{\text{refl}} = \frac{e^{-jk(r+2F)}}{r} \cdot \frac{1}{2}\sin\frac{\theta_s}{2}\left(1 - \sin\frac{\theta_s}{2}\right) \cdot \frac{1}{\pi}\int_0^{2\pi}\left[\hat{\phi}'E_{\theta_f}(\theta_s, -\psi) - \hat{\theta}'E_{\phi_f}(\theta_s, -\psi)\right]d\psi \tag{3.44}$$

with $\hat{\phi}'$ and $\hat{\theta}'$ defined in (3.33) and (3.34) respectively. Equation (3.44) can be further simplified if the feed patterns are known. Two examples are given in the following.

3.2.1 The point source model (3.22)

Using the feed model (3.22), one can calculate the integral in (3.44) and obtain

$$\mathbf{E}^{\mathrm{fr}}_{\mathrm{refl}} = \hat{p} \cdot \frac{e^{-jk(r+2F)}}{r} \cdot \frac{1}{2} \sin\frac{\theta_s}{2} \left(1 - \sin\frac{\theta_s}{2}\right) \cdot [A(\theta_s) - B(\theta_s)] \qquad (3.45)$$

where the polarization vector $\hat{p}$ are identical with that appears in the axial PO field (3.24). The validity of (3.45) has been justified by comparing with numerical integration. For example, using the antenna configuration $D = 10\lambda$, $F = 5\lambda$, and an x-polarized $\cos^q\theta$ feed with $q_1 = 4.3$, and $q_2 = 2.8$, one obtains the axial PTD fringe field $\mathbf{E}^{\mathrm{fr}}_{\mathrm{refl}} = -\hat{x}0.877 \times 10^{-8}\mathrm{volts}/\lambda$ at the point $\hat{r} = \hat{z}10^6\lambda$. It is observed that the amplitude of the axial fringe field (3.45) has k^0-dependence. To illustrate this feature, a paraboloidal reflector with $D = 1$ m and $F/D = 0.4$ is analyzed over a frequency band, and the result is compared with the axial PO field in Figure 3.3. Notice that the relative smallness of the fringe field is mainly due to the "difference" characteristics embedded in the factor $[A(\theta_s) - B(\theta_s)]$ of (3.45).

3.2.2 For circularly symmetric incident field

It is obvious from (3.44) that for circularly symmetric incident field ($E_{\theta_f} = E_{\phi_f}$) the EEW's cancel with each other and result in a vanishing axial fringe field.

3.2.3 For a prescribed TEM type incident field

Assume that the TEM-launcher produces on the edge of the reflector an incident field that is tangential to the edge of the reflector. Furthermore, for simplicity, let us assume that this tangential incident field possesses the symmetry that the field

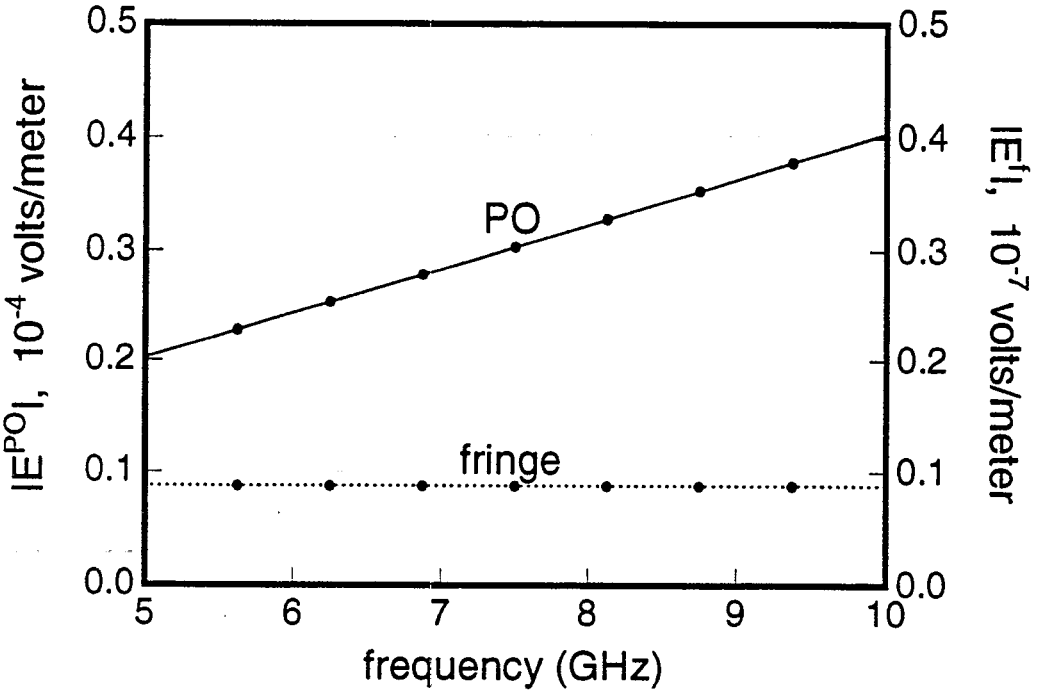

Figure 3.3: Absolute values of the amplitudes of the axial PO field and the axial fringe field for a paraboloidal reflector with $D = 1$ m and $F/D = 0.4$ using an x-polarized $\cos^q \theta$ feed with $q_1 = 4.3$, and $q_2 = 2.8$. Lines: closed-form formulas, dots: numerical integration.

on the $\psi \in [\pi, 2\pi]$ portion of the edge is the mirror image of that on the $\psi \in [0, \pi]$ portion, including the polarizations. In this situation, (3.44) reduces to

$$\mathbf{E}^{\mathrm{fr}}_{\mathrm{refl}} = \frac{e^{-jk(r+2F)}}{r} \cdot \frac{1}{2} \sin\frac{\theta_s}{2} \left(1 - \sin\frac{\theta_s}{2}\right) \cdot \frac{2}{\pi} \int_0^{\pi} E_{\phi_f}(\theta_s, \psi) \cos\psi d\psi \cdot \hat{y} \quad (3.46)$$

Notice that the fringe field vanishes if the pattern function E_{ϕ_f} is circularly symmetric. In other cases, the integral in the above equation has to be evaluated using a prescribed pattern function. Formulas for other TEM-launcher configurations can be obtained using a similar procedure, as long as the symmetry and the pattern functions can be properly identified. One may find discussions on the characteristics of a TEM feed in, for example, [9].

Chapter 4

Analysis of the transverse blades

In addition to the effect of the reflector rim diffraction studied and presented in a previous chapter, we investigate the diffraction effect of the spherical TEM-launcher's blades in this chapter for purpose of characterizing the axial field of a TEM-fed paraboloidal reflector antenna.

4.1 Classification of the blades

For convenience of discussion, let us first identify two ways that the blades may be placed: the "transverse" case and the "parallel" case. These two geometries can be distinguished from a front-view of the reflector as shown in Figure 4.1. In the transverse case, the projections of the blades on the reflector aperture reach maximum. In the parallel case, the projections reach minimum (straight line segments, precisely). The diffracted field for these two types of blades need separate considerations. Multiple diffractions and interactions between the reflector and the blades are not included.

- *The transverse case:*

  With the assumption of a local plane wave impinging on the blades, the GO field of the reflector+blades system is singular because, even with all the rays

that hit the blades blocked, there are still infinitely many rays traveling along the axial (caustic) direction. The diffracted field along the axial direction caused by the blades is vanishing in general. The exception occurs when the edges of the blades are so placed that the axial direction sits on the Keller's cone. In that situation, there are infinitely many diffraction points along the blade edges, and hence a singular diffracted field is resulted. These considerations reveal the difficulty of using GTD type analysis for the transverse blades.

On the other hand, since the PO current on the blade faces and the incident fields on the blade edges are well defined based on the assumption of an impinging plane wave, one may construct the PO/PTD scattered field in a straightforward manner.

- *The parallel case:*

  The PO/PTD analysis is not as applicable in the parallel case because the combination of grazing incidence and observation along the grazing diffracted ray results in the "Ufimtsev singularity" situation, in which the PTD diffraction coefficients become singular.

  As for GTD analysis, a consideration on the blade geometry and the situation of edge-on incidence shows that observation made along the axial direction is on the incident and reflection shadow boundaries of both edges of each blade. This demands the use of uniform theories in order to avoid the shadow boundary singularities pertaining to the GTD diffracted field. Even when this is done, the usefulness of the resultant diffracted field is diminished by the singular GO field.

It is seen that the PO/PTD technique can be applied to analyzing the transverse blade, while neither PO/PTD nor uniform GTD's are easily applicable to the parallel

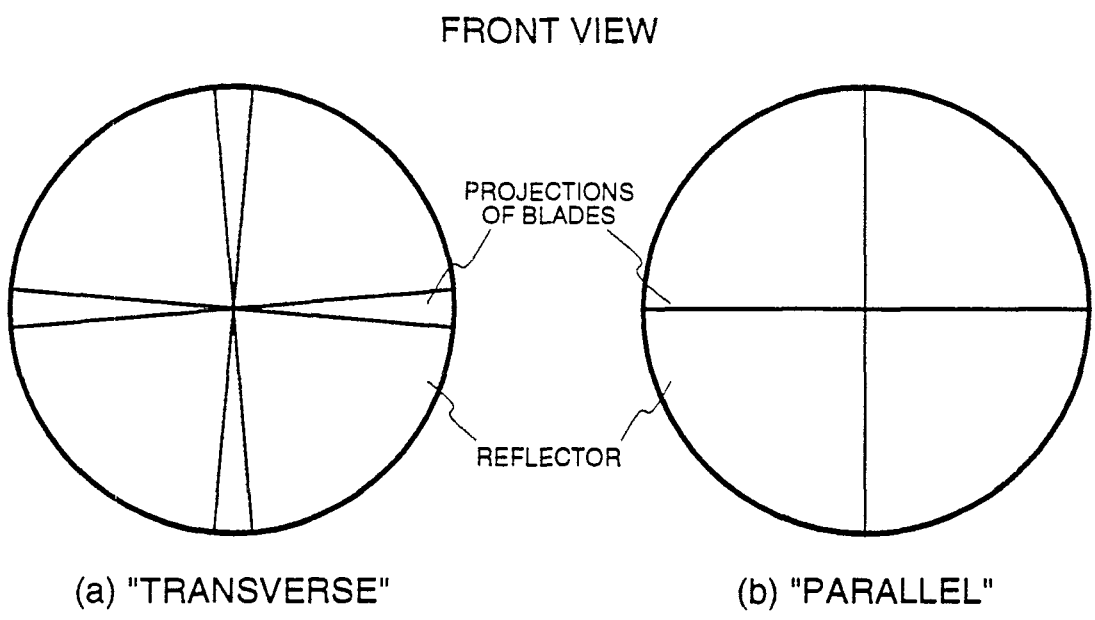

Figure 4.1: Two ways to place the blades: (a) the "transverse" case, (b) the "parallel" case.

blades. We present the PO/PTD analysis of the transverse blades in this report. The goal is to obtain closed-form formulas for the PO field and the PTD fringe field scattered from the blades.

4.2 Geometry of the transverse blades

Consider a paraboloidal reflector with diameter D and focal length F as shown in Figure 4.2. Assume that the condition $D < 4F$ is satisfied since a deep reflector is not typically used with a TEM-launcher feed. For a point P_0 on the edge of the reflector, let us define the *plane of the blade* as the plane which contains the line segment $\overline{OP_0}$ and the tangent of the reflector rim at P_0. Next, let us imagine a cylinder having the z-axis as its axis and a diameter D. We call this cylinder the "θ_s-cylinder", since it contains the collection of the rays that are launched from the focal point at an angle θ_s with respect to the negative z-axis and reflected by the paraboloid (see Figure 4.2). The intersection of the θ_s-cylinder and the blade plane is an ellipse. A transverse

blade is the portion of the intersection ellipse that subtends an angle ψ_h on each side of the line segment $\overline{OP_0}$. The curved edge of the blade is called the θ_s-arc.

It is seen that the geometry of a blade can be completely determined by specifying the point P_0 (which corresponds to the aperture angle ψ as shown in Figure 4.2), and the half angle of the blade, ψ_h. It is not difficult to see that the blade is enclosed in a (typically thin) isosceles triangle $P_1 - O - P_2$ where P_1 and P_2 are situated on the tangent of the reflector rim and symmetric to P_0. The acute angle of the isosceles triangle is situated on the focal point of the paraboloidal reflector, and the bisector of the acute angle passes through the reflector rim at P_0. The half length of the base of the isosceles triangle, d, is a convenient parameter that is related to the blade half angle by

$$d = r_0 \tan \psi_h \tag{4.1}$$

where r_0 is the focus-to-rim distance defined in (3.35).

It is convenient for later discussion to identify the coordinates of the points P_0, P_1, and P_2:

$$P_0 = \hat{x}\frac{D}{2}\cos\psi + \hat{y}\frac{D}{2}\sin\psi + \hat{z}z_0 \tag{4.2}$$

$$P_1 = \hat{x}\left(\frac{D}{2}\cos\psi + d\sin\psi\right) + \hat{y}\left(\frac{D}{2}\sin\psi - d\cos\psi\right) + \hat{z}z_0 \tag{4.3}$$

$$P_2 = \hat{x}\left(\frac{D}{2}\cos\psi - d\sin\psi\right) + \hat{y}\left(\frac{D}{2}\sin\psi + d\cos\psi\right) + \hat{z}z_0 \tag{4.4}$$

where z_0, the common z-coordinate of the reflector rim points, has been defined in (3.27). All the points on the blade share the same unit normal vector:

$$\hat{n} = \hat{x}\left(-\frac{m_-}{m_+}\cos\psi\right) + \hat{y}\left(-\frac{m_-}{m_+}\sin\psi\right) + \hat{z}\left(-\frac{D/2F}{m_+}\right) \tag{4.5}$$

which is pointing toward the reflector, and useful in the construction of the PO current.

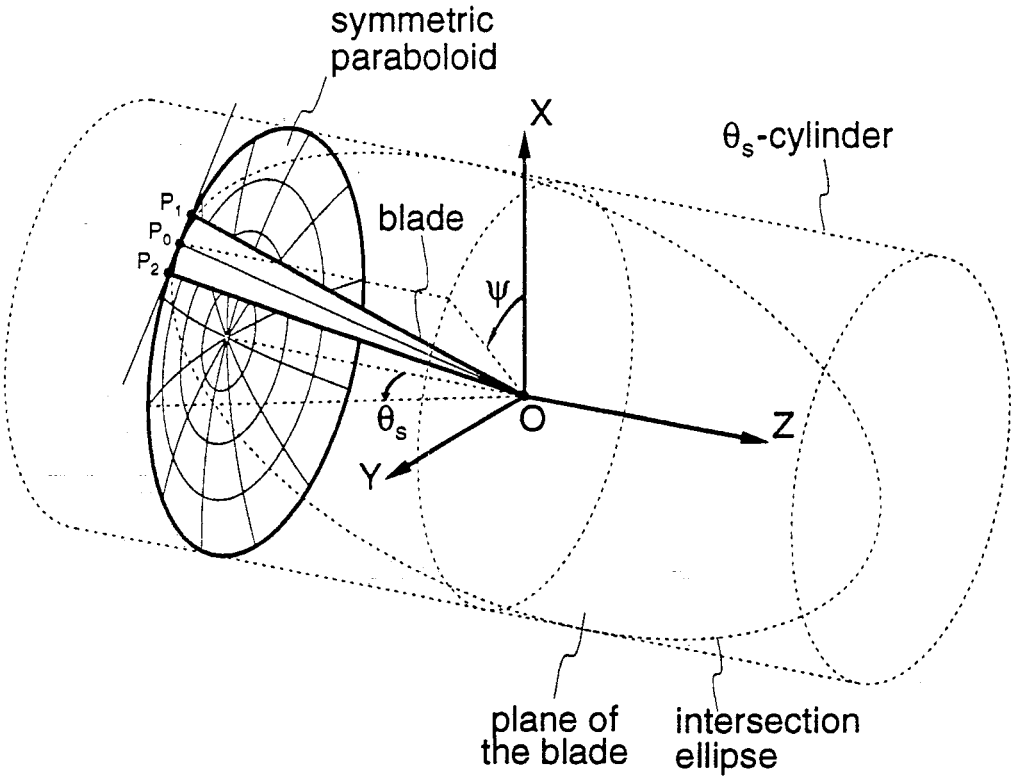

Figure 4.2: Geometry of a transverse blade.

4.3 The incident field

The field incident on the blades must be assumed before one can calculate the PO field and the PTD fringe field of the blades. In this report, we assume a feed (primary) field and calculate the field reflected by the reflector using Geometrical Optics (GO) analysis. This reflected (secondary) field, which is found to have a uniform phase front, are taken as the incident field on the blades.

Precisely, if we assume the feed fields:

$$\mathbf{E}^{\text{feed}} = \frac{e^{-jkr_f}}{r_f}\left(\hat{\theta}_f E_{\theta_f} + \hat{\phi}_f E_{\phi_f}\right) \tag{4.6}$$

then the reflected field at the point $(\rho, \phi, z) = (r_f \sin\theta_f, \phi, z)$ as obtained from GO

analysis is

$$\begin{bmatrix} E_x^{\text{inc}} \\ E_y^{\text{inc}} \end{bmatrix} = \frac{e^{-jk(z+2F)}}{r_f} \begin{bmatrix} -\cos\phi & -\sin\phi \\ -\sin\phi & \cos\phi \end{bmatrix} \begin{bmatrix} E_{\theta_f} \\ E_{\phi_f} \end{bmatrix}, \quad E_z^{\text{inc}} = 0 \qquad (4.7)$$

Notice that the superscript "inc" in (4.7) is used to denote the field incident on the blade instead of the reflector, and the distance r_f is a function of θ_f:

$$r_f = \frac{2F}{1+\cos\theta_f} \qquad (4.8)$$

In a previous chapter the feed model (3.22) has been used to determine the PO and fringe field from the reflector. Substituting this model into (4.7) one finds that the depolarization effect produces a complicated expression for the incident field on the blades. This complication can be avoided if one assumes a symmetric feed pattern, namely,

$$A(\theta_f) = B(\theta_f) \qquad (4.9)$$

The assumption (4.9) will be used throughout the rest of this report because it simplifies the analysis and facilitates extracting useful information from the results. Nevertheless, (4.9) is not so restrictive as it may appear to be. It is not only because the TEM-launchers produce rather symmetric field patterns, but also because the half angle of a blade is usually as small as several degrees, within which the asymmetric feed pattern can not be experienced completely. In other words, a blade sees only the portion of the field pattern that is "local" to its vicinity, and hence the application of a symmetric pattern that mimics the field in the blade's vicinity becomes a good approximation. Using (4.9) and (3.22) in (4.7) and recalling the transformation (3.4), one obtains

$$\mathbf{E}^{\text{inc}} = -\hat{p}\frac{e^{-jkr_f}}{r_f}A(\theta_f) \qquad (4.10)$$

$$\mathbf{H}^{\text{inc}} = \frac{1}{Z_0}\hat{z}\times\mathbf{E}^{\text{inc}} \qquad (4.11)$$

where the polarization vector $\hat{p}$ is defined in (3.24). Equations (4.10) and (4.11) are the assumed equations of the incident field on the blades.

4.4 The axial PO field of a transverse blade

Using the incident magnetic field (4.11), one may write the PO field (2.17) as

$$\mathbf{E}^{\text{PO}}_{\text{blade}} = \hat{p} \cdot \frac{e^{-jk(r+2F)}}{4\pi r} \cdot jk \sin\theta_s \cdot \frac{1}{F} \int_{\text{blade}} A(\theta_f)(1+\cos\theta_f)\, d\Sigma \qquad (4.12)$$

where θ_s is the subtended angle of the reflector (see Figure 4.2) as defined in (3.21). In order to further reduce the PO field, let us parameterize the blade using the parameter $t \in [0,1]$ in the manner that $t = 0$ corresponds to the tip of the blade and $t = 1$ to the curved edge of the blade. More precisely, we relate each t value to an arc, the "θ_f-arc", which is the intersection of the blade and the "θ_f-cylinder". The θ_f-cylinder is an imagined cylinder that has z-axis as its axis, and contains the collection of the rays that are launched from the focal point at an angle θ_f with respect to the negative z-axis and reflected by the paraboloid. The parameter t and the angle θ_f are related by

$$\theta_f = 2\arctan\frac{Dt}{4F} \qquad (4.13)$$

It is seen from this equation that

$$\theta_f : 0 \rightarrow \theta_s \quad \text{as} \quad t : 0 \rightarrow 1 \qquad (4.14)$$

The reason of using this parameterization is that for each t value, the angle θ_f is constant, and therefore the two-dimensional integral in (4.12) can be reduced to an one-dimensional integral. We elaborate on this reduction in the following.

Let us set up a ρ_b-axis that starts off from the tip of the blade, O, and follows the bisector of the blade as shown in Figure 4.3. The variable ρ_b is related to t by

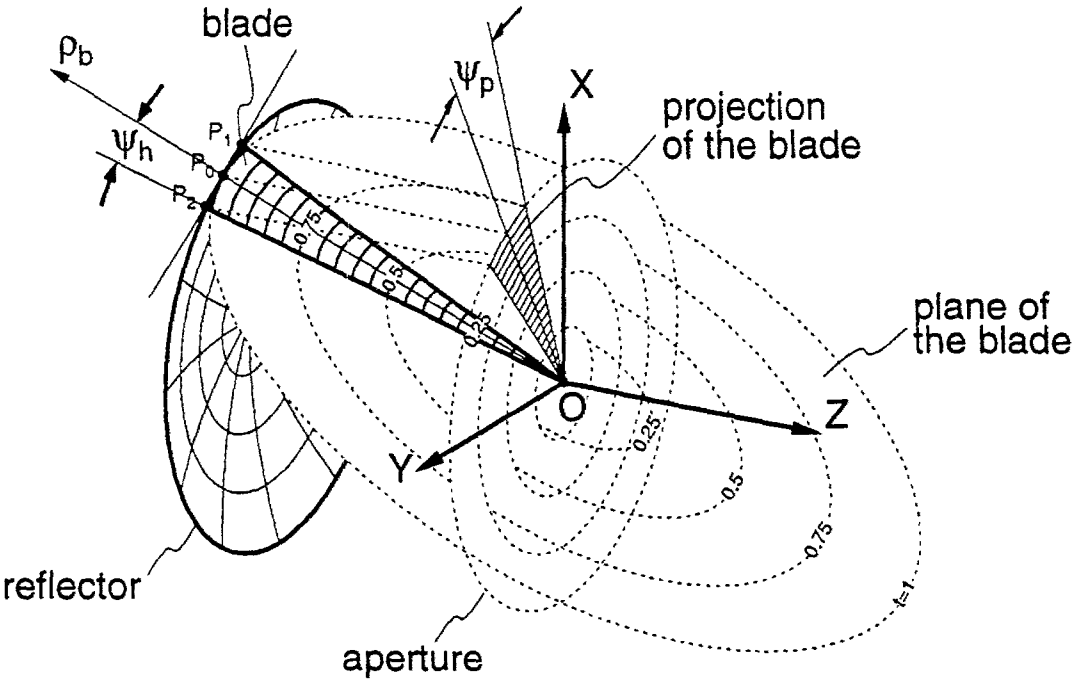

Figure 4.3: Parameterization of a transverse blade.

$$\rho_b = \frac{Dt}{2\sin\theta_s} \tag{4.15}$$

Next, let us define a function $L(\psi_h;\theta_s)$, which gives the arc length between $[-\psi_h,\psi_h]$ for an ellipse with semi-axes 1 and $\sin\theta_s$ as shown in Figure 4.4. With these definitions, one finds immediately that the length of a θ_f-arc is given by $\rho_b \cdot L(\psi_h;\theta_s)$, and the area element $d\Sigma$ can be cast into

$$d\Sigma = \left(\frac{D}{2\sin\theta_s}\right)^2 L(\psi_h;\theta_s)\, t\, dt \tag{4.16}$$

Notice that integrand of the integral in (4.12) is expressed as a function of the variable θ_f; it is convenient to rewrite dt as

$$dt = \frac{4F}{D}\cdot\frac{d\theta_f}{1+\cos\theta_f} \tag{4.17}$$

with the help of (4.13). Inserting (4.16) and (4.17) into (4.12), one reaches the final

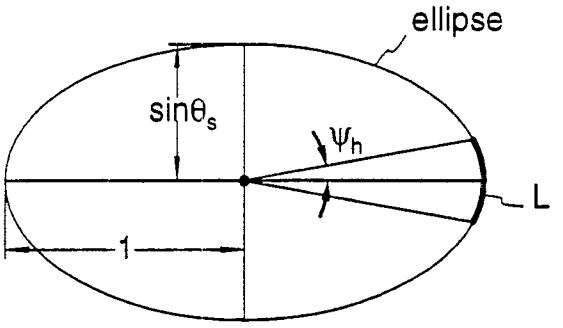

Figure 4.4: Definition of the function $L(\psi_h;\theta_s)$.

form of the PO field scattered from a blade:

$$\mathbf{E}^{\mathrm{PO}}_{\mathrm{blade}} = \hat{p}\cdot\frac{e^{-jk(r+2F)}}{r}\cdot(jkF)\cdot f(\psi_h;\theta_s)\cdot 2\int_{\cos\theta_s}^{1}\frac{A(\theta_f)}{1+\cos\theta_f}\,d\cos\theta_f \quad (4.18)$$

with

$$f(\psi_h;\theta_s) \equiv \frac{L(\psi_h;\theta_s)}{2\pi\sin\theta_s} > 0 \quad (4.19)$$

Comparing (4.18) with the PO field (3.23) of a reflector with symmetric feed patterns:

$$\mathbf{E}^{\mathrm{PO}}_{\mathrm{refl}} = \hat{p}\cdot\frac{e^{-jk(r+2F)}}{r}\cdot(-jkF)\cdot 2\int_{\cos\theta_s}^{1}\frac{A(\theta_f)}{1+\cos\theta_f}\,d\cos\theta_f \quad (4.20)$$

It is clear that the PO field of the blade tries to cancel that of the reflector in a fraction determined by the function $f(\psi_h;\theta_s)$. This is a manifestation of the "blockage" or "shadowing" effect of the blade. In a conventional treatment of the blockage in PO analysis, the current on the reflector surface that is under the projection (or, the shadow) of the blade is set to zero. It is interesting to calculate the amount of blockage predicted by (4.18), and compare it with the conventional treatment. To achieve this, let us write the exact form of the function $f(\psi_h;\theta_s)$:

$$f(\psi_h;\theta_s) = \frac{1}{\pi}\int_0^{\psi_h}\frac{\sqrt{\sin^2\psi+\sin^4\theta_s\cos^2\psi}}{\left(\sqrt{\sin^2\psi+\sin^2\theta_s\cos^2\psi}\right)^3}\,d\psi \quad (4.21)$$

and plot it in Figure 4.5. When $\psi_h \ll 1$, which is almost always the case, $f(\psi_h;\theta_s)$

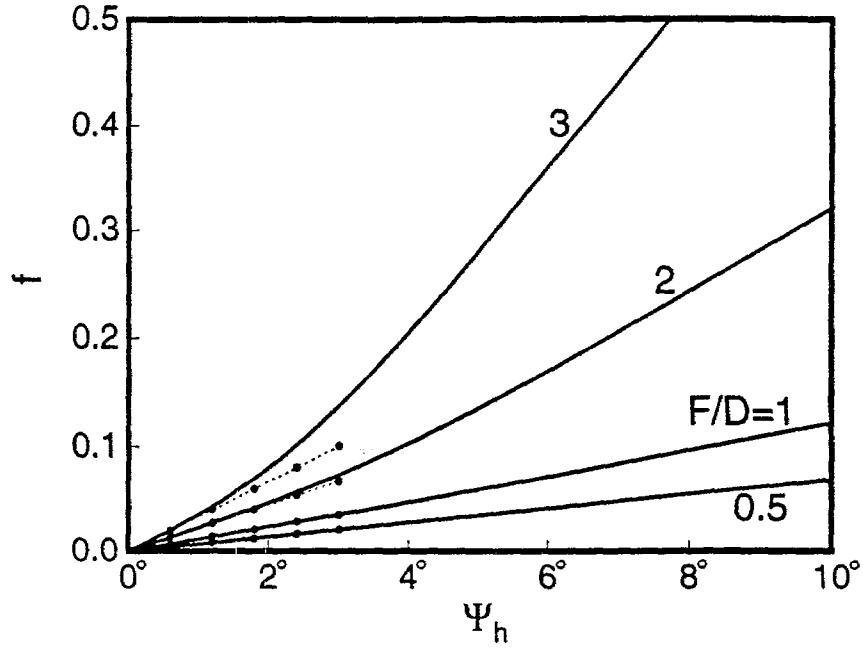

Figure 4.5: The function $f(\psi_h;\theta_s)$ (solid lines) and its linear approximation (dots).

can be approximated by

$$f(\psi_h;\theta_s) \simeq \frac{\psi_h}{\pi \sin\theta_s} \tag{4.22}$$

As plotted in dotted lines in Figure 4.5, it is seen that (4.22) is a very good approximation when ψ_h is small (say, less than 5°) and when the F/D ratio of the reflector is not unreasonably large (less than 2, for example). Independently, however, one finds that the right side of (4.22) is exactly the ratio of the projection of the blade on the x-y plane to that of the reflector. These results provide a satisfactory justification for the conventional treatment of the blockage.

4.5 The fringe field of a transverse blade

The PTD fringe field of a transverse blade is constructed in this section. As a summary, we start with the determination of the local coordinate systems and the incident angles, which are used to the construct the diffraction coefficients. Using the diffrac-

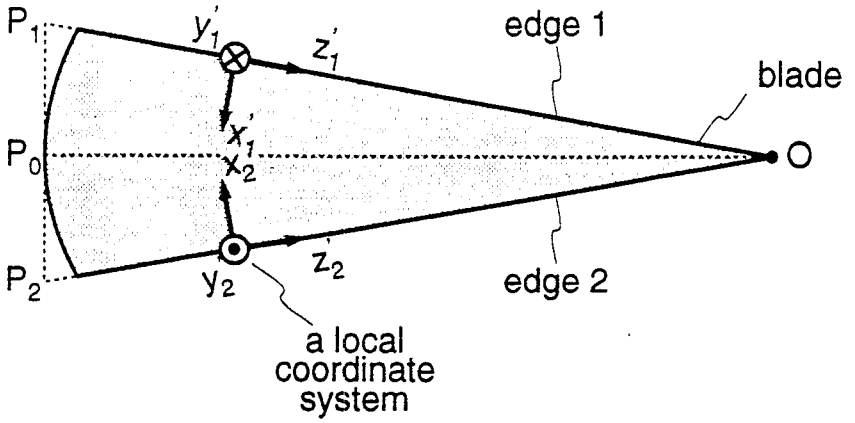

Figure 4.6: Local coordinate systems defined on the edges of a blade.

tion coefficients and the unit vectors associated with an axial observation point (in terms of the local coordinate systems), we are able to formulate the fringe field, and reach a simple closed-form formula. This procedure is presented in the following,

4.5.1 The local coordinate systems

The first step in calculating the PTD fringe field is to erect local coordinate systems along the edges of the scatterer. Figure 4.6 depicts one possible way of setting up the local coordinate systems for a transverse blade. Notice that based on our PTD formulation, it is required that the z'-axis is tangential to the edge of the blade, and the x'-axis is situated on the blade and pointing inward at a right angle to the edge. For convenience, let us call the local coordinate systems along edge 1 as $C_1' = \{\hat{x}_1', \hat{y}_1', \hat{z}_1'\}$, and that on edge 2 as $C_2' = \{\hat{x}_2', \hat{y}_2', \hat{z}_2'\}$. It is not difficult to formulate these local coordinate systems by inspecting Figure 4.6:

$$\hat{y}_1' = \hat{n}, \quad \hat{z}_1' = -\frac{\mathbf{OP}_1}{|\mathbf{OP}_1|}, \quad \hat{x}_1' = \hat{y}_1' \times \hat{z}_1' \tag{4.23}$$

$$\hat{y}_2' = -\hat{n}, \quad \hat{z}_2' = -\frac{\mathbf{OP}_2}{|\mathbf{OP}_2|}, \quad \hat{x}_2' = \hat{y}_2' \times \hat{z}_2' \tag{4.24}$$

Since the vector $\hat{n}$ and the position of the points P_1 and P_2 have been found in (4.5), (4.3), and (4.4) respectively, the local coordinate systems are therefore determined.

4.5.2 The incident angles and observation angles

In order to construct the diffraction coefficients, we must first calculate the incident angles and observation angles. For that purpose, let us recall that the incident field on the blade has been modeled as a plane wave that travel along the z-axis. The incident angles are determined by the relative orientation of the incident rays and the local coordinate systems. Precisely, the following procedure:

$$\hat{r}_i = -\hat{z} \tag{4.25}$$

$$\cos\theta'_{i,1} = \hat{r}_i \cdot \hat{z}'_1, \quad \tan\phi'_{i,1} = \frac{\hat{r}_i \cdot \hat{y}'_1}{\hat{r}_i \cdot \hat{x}'_1} \tag{4.26}$$

$$\cos\theta'_{i,2} = \hat{r}_i \cdot \hat{z}'_2, \quad \tan\phi'_{i,2} = \frac{\hat{r}_i \cdot \hat{y}'_2}{\hat{r}_i \cdot \hat{x}'_2} \tag{4.27}$$

leads to the solution:

$$\theta'_{i,1} = \theta'_{i,2} = \arccos\left(-\frac{m_-}{m_d}\right) \tag{4.28}$$

$$\phi'_{i,1} = 2\pi - \phi'_{i,2} = \arctan\left(\frac{\cot\psi_p}{-\cos\phi'_{i,1}}\right) \tag{4.29}$$

where the angle ψ_p as defined by

$$\psi_p = \arctan\left(\frac{2d}{D}\right) \tag{4.30}$$

is the half angle of the blade's projection on the x-y plane, as Figure 4.3 shows. For example, if $F/D = 1$ and $d/F = 0.1$, one has $\theta'_{i,1} = \theta'_{i,2} = 151.458°$, $\phi'_{i,1} = 80.035°$, and $\phi'_{i,2} = 279.965°$.

Since the observation are made along the z-axis, which is the same as the direction of the incident ray, one obtains the observation angles immediately:

$$\theta'_1 = \pi - \theta'_{i,1}, \quad \phi'_1 = \phi'_{i,1} + \pi \tag{4.31}$$

$$\theta'_2 = \pi - \theta'_{i,2}, \quad \phi'_2 = \phi'_{i,2} + \pi \tag{4.32}$$

4.5.3 The diffraction coefficients

Have found the incident angles, one may apply them in (2.8), (2.9), and (2.10). The results are

$$F_{\theta,1} = F_{\theta,2} = -\tan\frac{\phi'_{i,1}}{2} \tag{4.33}$$

$$G_{\theta,1} = -G_{\theta,2} = -2\cos\theta'_{i,1} \tag{4.34}$$

$$G_{\phi,1} = G_{\phi,2} = -\tan\frac{\phi'_{i,1}}{2} \tag{4.35}$$

These formulas have been validated by comparing with the results obtained from direct numerical evaluation of the definitive formulas (2.8), (2.9), and (2.10). In order to construct the fringe field, we need to collect one last piece of information: the unit vectors $\hat{\theta}'$'s and $\hat{\phi}'$'s associated with observation points along the antenna axis, in view of the local coordinate systems.

4.5.4 Unit vectors associated with axial observation

The unit vectors $\hat{\theta}'$'s and $\hat{\phi}'$'s can be constructed with the Cartesian-to-spherical transformations:

$$\hat{\theta}' = \hat{x}'\cos\theta'\cos\phi' + \hat{y}'\cos\theta'\sin\phi' - \hat{z}'\sin\theta' \tag{4.36}$$

$$\hat{\phi}' = -\hat{x}'\sin\phi' + \hat{y}'\cos\phi' \tag{4.37}$$

using the known Cartesian unit vectors (4.23), (4.24) and the observation angles (4.31), (4.32). As a result, one finds that

$$\hat{\theta}'_1 = \hat{x}\cos(\psi - \psi_p) + \hat{y}\sin(\psi - \psi_p) \tag{4.38}$$

$$\hat{\phi}'_1 = -\hat{x}\sin(\psi - \psi_p) + \hat{y}\cos(\psi - \psi_p) \tag{4.39}$$

$$\hat{\theta}'_2 = \hat{x}\cos(\psi + \psi_p) + \hat{y}\sin(\psi + \psi_p) \tag{4.40}$$

$$\hat{\phi}'_2 = -\hat{x}\sin(\psi + \psi_p) + \hat{y}\cos(\psi + \psi_p) \tag{4.41}$$

Now we are in the position to construct the PTD fringe field for a transverse blade.

4.5.5 The fringe field

The fringe field of the blade is the sum of the fringe field from edge 1, denoted by $\mathbf{E}^{\mathrm{fr},1}_{\mathrm{blade}}$, and that from edge 2, $\mathbf{E}^{\mathrm{fr},2}_{\mathrm{blade}}$:

$$\mathbf{E}^{\mathrm{fr}}_{\mathrm{blade}} = \mathbf{E}^{\mathrm{fr},1}_{\mathrm{blade}} + \mathbf{E}^{\mathrm{fr},2}_{\mathrm{blade}} \tag{4.42}$$

Each of the fringe field components is constructed by an integration of the equivalent edge currents (composed of the incident field and the diffraction coefficients) along the corresponding edge of the blade. Since all the ingredients involved in each "edge"-integral have been determined, the evaluation of these integrals are straightforward. The details of this procedure is tedious and is omitted here. Combining the resultant formulas, one obtains for the observation point $z = r$:

$$\mathbf{E}^{\mathrm{fr}}_{\mathrm{blade}} = \hat{p}^{\mathrm{fr}} \cdot \frac{e^{-jk(r+2F)}}{r} \cdot \sin\theta'_{i,1} \left(\cos\phi'_{i,1} + \cos 2\psi_p\right) \cdot \frac{1}{2\pi} \int_0^{\theta_s} A(\theta_f) d\theta_f \tag{4.43}$$

where the angle ψ_p has been defined in (4.30) and the polarization angle $\hat{p}^{\mathrm{fr}}$ is given by

$$\hat{p}^{\mathrm{fr}} = \begin{cases} \hat{x}\cos 2\psi + \hat{y}\sin 2\psi, & \text{x-pol feed} \\ -\hat{x}\sin 2\psi + \hat{y}\cos 2\psi, & \text{y-pol feed} \\ \frac{\hat{x}-j\hat{y}}{\sqrt{2}} e^{j2\psi}, & \text{RHCP feed} \\ \frac{\hat{x}+j\hat{y}}{\sqrt{2}} e^{-j2\psi}, & \text{LHCP feed} \end{cases} \tag{4.44}$$

Notice that 2ψ-dependence of the polarization vector. This is resulted from the summation of the two fringe field components. For the same reason, the sense of circular polarization has also been inverted compared to that of the PO field (4.18), (3.24).

Chapter 5

Conclusions

The radiated field along the axial direction of a TEM-fed symmetric paraboloid reflector antenna is studied using the techniques of Physical Optics (PO) and Physical Theory of Diffraction (PTD). As a result, with a general spherical incident field representation (3.22), closed-form formulas are derived for

- the PO field of the reflector (3.23),
- the PTD fringe field from the edge of the reflector (3.45),
- the PO field of a transverse blade (4.18), and
- the PTD fringe field of a transverse blade (4.43).

Specialization of these general results to a prescribed incident field generated by the TEM-launcher is also considered (3.46). The parallel blades are not treated in this report due to complications involved in the PO/PTD and GO/GTD high frequency diffraction techniques. We propose conducting hybrid method such as the POHM (Physical Optics Hybrid method) in the continuation of this work.

Appendix A

Comparison of the axial field formulas: paraboloid versus disc

A paraboloid becomes less curved as its focal length F increases; for large F, it tends to be a flat disc. In this situation, the axial PO field (3.23) of a paraboloid, shall be similar to that of a circular disc. Fortunately, a closed-form formula for the axial field of a circular disc with uniformly distributed surface current has been derived previously [10]. This formula is valid for both near- and far-field observations. In this appendix, we will specialize the disc formula to far-field observation and compare with (3.23) for large F. This comparison serves as a justification of the validity of these independently derived formulas.

The geometry of a circular disc is depicted in Figure A.1, in which the uniformly current is y-oriented. The closed-form formula for the axial field of the disc is [10]

$$\begin{aligned}\mathbf{E}^{disc} &= \hat{y}\frac{Z_0 J_y}{2}\left\{\left(\frac{1}{jkz}-1\right)e^{-jkz}+\right.\\ &\left.\frac{1}{z^2+a^2}\left[z^2+\frac{z^2}{jk\sqrt{z^2+a^2}}-\frac{2\sqrt{z^2+a^2}}{jk}\right]e^{-jk\sqrt{z^2+a^2}}\right\} \qquad \text{(A.1)}\end{aligned}$$

where a is the radius of the disc, and J_y represents the current. Notice that this formula is valid everywhere along the z-axis, including the near and the far-field. For purpose of comparison, let us simplify (A.1) for far-field observation:

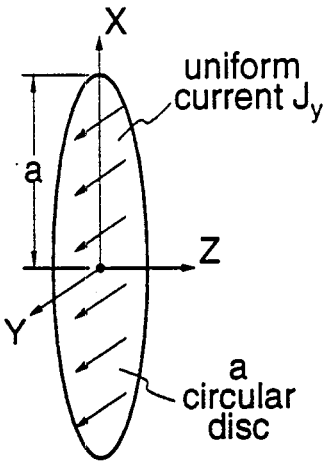

Figure A.1: Geometry of a circular disc with uniformly distributed surface current.

$$\begin{aligned}
\mathbf{E}^{disc} \quad & \overset{z \gtrsim a}{\sim} \quad \hat{y}\frac{Z_0 J_y}{2}\left[\left(\frac{1}{jkz}-1\right)e^{-jkz}+\frac{1}{z^2}\left(z^2+\frac{z}{jk}-\frac{2z}{jk}\right)e^{-jk(z+a^2/2z)}\right] \\
& = \quad \hat{y}\frac{Z_0 J_y}{2}\left(\frac{1}{jkz}-1\right)e^{-jkz}\left(1-e^{-jka^2/2z}\right) \\
& \overset{z \gg ka^2/2}{\sim} \quad \hat{y}\frac{Z_0 J_y}{2}\left(1-\frac{1}{jkz}\right)e^{-jkz}\left(-j\frac{ka^2}{2z}\right) \\
& \overset{kz \gtrsim 1}{\sim} \quad \hat{y}J_y \cdot \left(-jZ_0\frac{ka^2}{4z}\right)\cdot e^{-jkz}
\end{aligned} \tag{A.2}$$

For a paraboloid with large focal length F, the approximations

$$A(\theta_f) \sim B(\theta_f) \sim 1, \quad \theta_s \ll 1 \tag{A.3}$$

can be applied to (3.23), and the result is

$$\mathbf{E}^{\mathrm{PO}}_{\mathrm{refl}} \sim \hat{y}jkF\frac{e^{jk(r+2F)}}{r}\cdot\frac{D^2}{8F^2} \tag{A.4}$$

On the other hand, the PO current (3.17) produced by a y-polarized feed (3.22) is found to be

$$\mathbf{J}^{\mathrm{PO}} = \hat{y}J_y = \hat{y}\left(-\frac{2}{Z_0}\cdot\frac{e^{-jkF}}{F}\right) \tag{A.5}$$

for large F. Combining (A.4) and (A.5), one obtains

$$\mathbf{E}_{\text{refl}}^{\text{PO}} \sim \hat{y} J_y \cdot \left(-jZ_0 \frac{ka^2}{4r} \right) \cdot e^{-jk(r+F)} \tag{A.6}$$

Now we are in the position to compare the formulas for the disc (A.2) and the paraboloid (A.6). One observes that the apparently different phase terms, e^{-jkz} and $e^{-jk(r+F)}$, are actually identical because the origins of the coordinate systems in Figure 3.1 and Figure A.1 are offset by a distance F. Secondly, notice that although the decay factors $1/z$ and $1/r$ are different due to the different coordinate system origins, the difference between them becomes indiscernible at far distance $r \gg F$. Therefore we may conclude that the formulas for the disc (A.2) and the paraboloid (A.6) are consistent with each other.

Acknowledgements

The authors wish to thank Dr. C. Baum and Dr. D. Giri for their constructive suggestions during the preparation of this report.

Bibliography

[1] A. Michaeli. "Elimination of infinities in equivalent edge currents, part I: Fringe current components". *IEEE Trans. Antennas Propagat.*, AP-34(7):912–918, July 1986.

[2] P. Ya. Ufimtsev. "Elementary edge waves and the physical theory of diffraction". *Electrmagn.*, 11(2):125–160, April-June 1991.

[3] D. W. Duan, Y. Rahmat-Samii, and J. P. Mahon. "Scattering from a circular disc: a comparative study of PTD and GTD techniques". *IEEE Proc.*, 79(10):1472–1480, October 1991.

[4] W. V. T. Rusch. "Physical-Optics diffraction coefficients for a paraboloid". *Electr. Lett.*, 10(17):358–360, August 1974.

[5] C. M. Knop. "An extension of Rusch's asymptotic Physical Optics diffraction theory of a paraboloid antenna". *IEEE Trans. Antennas Propagat.*, AP-23(5):741–743, September 1975.

[6] M. Safak. "Calculation of radiation patterns of paraboloidal reflectors by high-frequency asymptotic techniques". *Electr. Lett.*, 12(9):229–231, April 1976.

[7] Y. Rahmat-Samii. "Reflector antennas". In Y. T. Lo and S. W. Lee, editors, *"Antenna Handbook"*, chapter 15. Van Nostrand Reinhold Company, New York, 1988.

[8] I. M. Ryshik and I. S. Gradstein. *"Tables of series, products, and integrals"*. Deutscher Verlag der Wissenschaften, 2nd edition, 1963.

[9] C. E. Baum and E. G. Farr. "Impulse radiating antennas". In H. L. Bertoni, L. Carin, and L. B. Felsen, editors, *Ultra-Wideband, Short-Pulse Electromagnetics*, pages 139–147. WRI, Polytechnique University, Brooklyn, New York, Plenum Press, January 1993.

[10] V. Galindo-Israel and Y. Rahmat-Samii. "A new look at Fresnel field computation using the Jacobi-Bessel series". *IEEE Trans. Antennas Propagat.*, AP-29(6):885–898, November 1981.